European Journal of Medicinal Chemistry 45 (2010) 5140–5149

Contents lists available at ScienceDirect

European Journal of Medicinal Chemistry

journal homepage: http://www.elsevier.com/locate/ejmech

Original article

Exploring new inhibitors of *Plasmodium falciparum* purine nucleoside phosphorylase

Huaqing Cui [a,b], Gian Filippo Ruda [b], Juana Carrero-Lérida [a], Luis M. Ruiz-Pérez [a], Ian H. Gilbert [b,*], Dolores González-Pacanowska [a,**]

[a] *Instituto de Parasitología y Biomedicina "López-Neyra", Consejo Superior de Investigaciones Científicas, Avda. del Conocimiento s/n, 18100-Armilla, Granada, Spain*
[b] *College of Life Sciences, University of Dundee, Sir James Black Centre, Dundee DD1 5EH, UK*

ARTICLE INFO

Article history:
Received 26 March 2010
Received in revised form
9 August 2010
Accepted 10 August 2010
Available online 14 August 2010

Keywords:
Malaria
Purine nucleoside phosphorylase
Uridine phosphorylase
Transition state inhibitor
Drug discovery

ABSTRACT

Plasmodium falciparum purine nucleoside phosphorylase (*Pf*PNP) has a central role in purine salvage and inhibitors of the enzyme have been shown to have antiplasmodial activity. The enzyme preferentially uses inosine as substrate ($K_m = 5$ μM, $k_{cat}/K_m = 7.4 \times 10^4$ M^{-1} s^{-1}), but can also use uridine, albeit less efficiently ($K_m = 85$ μM, $k_{cat}/K_m = 306$ M^{-1} s^{-1}). In an effort to identify new *Pf*PNP inhibitors, two series of compounds were prepared. Series **1** was based on known human uridine phosphorylase inhibitors whilst series **2** was uracil equivalents of purine-based PNP transition state inhibitors. These two series of compounds were assayed for inhibition of both *Pf*PNP activity and growth of *P. falciparum*. The transition state analogues were found to be moderate inhibitors of *Pf*PNP (most potent compound, $K_i = 6$ μM).

1. Introduction

It is estimated that malaria causes 300–500 million clinical cases and 2 million deaths annually [1]. *Plasmodium falciparum* is responsible for the majority of deaths due to malaria. Drug resistance is a major problem for treatment and there is a need for new drugs particularly those that have a new mode of action [2,3].

P. falciparum cannot synthesize purines *de novo*, and is entirely reliant on the salvage of extracellular purines. Therefore, the purine salvage pathway is a potential target for antimalarial chemotherapy [4]. An enzyme involved in this pathway is *P. falciparum* purine nucleoside phosphorylase (*Pf*PNP), which catalyzes the phosphorolysis of inosine to ribose-1-phosphate and hypoxanthine (Fig. 1). Uridine is also known to be a substrate for this *Pf*PNP, although the affinity ($K_m = 85$ μM, $k_{cat}/K_m = 306$ M^{-1} s^{-1}) is lower than for inosine ($K_m = 5$ μM, $k_{cat}/K_m = 7.4 \times 10^4$ M^{-1} s^{-1}) and the catalytic efficiency is 240-fold higher with the latter [5].

*Pf*PNP is essential for parasite survival. Thus targeted gene disruption in a *P. falciparum* strain in order to ablate PNP expression has resulted in parasites that exhibit growth defects at physiological concentrations of hypoxanthine and require exogenous purines for sustained growth [9]. Chemical validation of *Pf*PNP has also been performed and transition state analogues developed that inhibit hPNP and *Pf*PNP and kill *P. falciparum in vitro* [10].

Immucillin-H (**3**) (Fig. 2) is a PNP transition state analogue inhibitor, which inhibits hPNP very potently ($K_d = 56$ pM) and the *Plasmodium* enzyme *Pf*PNP ($K_i = 860$ pM) slightly less strongly [11]. Immucillin-H was designed using kinetic isotope measurements which allowed for the identification of the transition state [7,12]. The study indicated that catalysis proceeds via a classic S_N1 nucleophilic substitution reaction in which, at transition state, the ribose ring forms an oxocarbenium ion (Fig. 1) [8,13]. In these transition state inhibitors, oxygen is replaced by a basic nitrogen, which mimics the positive charge of the oxocarbenium ion, and the distance between the ribose and the base in Immucillin-H is 1.5 Å, which is very close to the distance between the ribose and the leaving base in the transition state [13]. The substrate specificity, catalytic site structure, and subunit structure of *Pf*PNP are distinct from hPNP [6]. Potentially this can be used to design inhibitors which are selective for *Pf*PNP over hPNP. However, most

Abbreviations: ADA, adenosine deaminase; BBB, 5-(*m*-benzyloxy)benzylbarbituric acid; BBBA, 1-[(2-hydroxyethoxy)methyl]-5-(*m*-benzyloxy)benzylbarbituric acid acyclonucleoside; NOESY, nuclear Overhauser effect spectroscopy; *Pf*PNP, *Plasmodium falciparum* purine nucleoside phosphorylase; MT-immH, 5′-methylthio-immucillin-H; UP, uridine phosphorylase.

* Corresponding author.
** Corresponding author. Tel.: +34 958181631; fax: +34 958181632.
E-mail addresses: i.h.gilbert@dundee.ac.uk (I.H. Gilbert), dgonzalez@ipb.csic.es (D. González-Pacanowska).

0223-5234/$ – see front matter © 2010 Elsevier Masson SAS. All rights reserved.
doi:10.1016/j.ejmech.2010.08.026

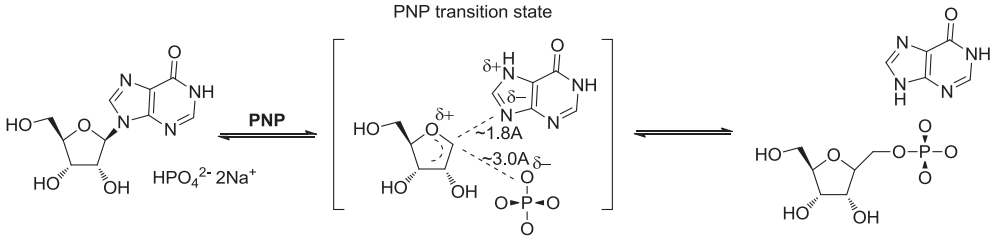

Fig. 1. Inosine phosphorylase catalyzed by purine nucleoside phosphorylase. The reaction is an S_{N1} type mechanism [6–8].

of the reported transition state inhibitors bind preferentially to hPNP rather than *Pf*PNP [5,10]. There are several exceptions to this: for example MT-immH (5′-methylthio-immucillin-H) gives the largest selectivity between *Pf*PNP and hPNP so far reported, a 100-fold difference between *Pf*PNP ($K_i = 2.7$ nM) and hPNP ($K_i = 303$ nM) [14]; although MT-immH still shows nanomolar potency against hPNP. It is proving challenging to obtain compounds that are highly selective towards *Pf*PNP. However, it should be noted that the antiparasitic activity of these PNP inhibitors may in part be due to simultaneous inhibition of hPNP, preventing generation of hypoxanthine by the erythrocytes [5,9,10].

In the study we report here, two series of compounds have been designed as potential inhibitors of *Pf*PNP. In particular, the fact that *Pf*PNP can use uridine as a substrate has been exploited.

First, human uridine phosphorylase (UP) has been considered as target for cancer therapy and many nucleoside analogues have been evaluated as inhibitors of the enzyme [15–17]. As *Pf*PNP shows significant activity with uridine and similarity to human uridine phosphorylase, a potent human uridine phosphorylase inhibitor 5-(*m*-benzyloxy)benzylbarbituric acid acyclonucleoside (BBBA **2**, $K_i = 1.1$ nM) [15] and its intermediate-5-(*m*-benzyloxy)benzylbarbituric acid (BBB **1**, $K_i = 2.3$ μM) [15] were made to test for activity against *Pf*PNP (Fig. 2). If active and selective, these could provide a starting point for a more focused discovery programme.

Second, different generations of purine-based transition state inhibitors of human and *Plasmodium* PNP have been reported [11,13,18]. Compound **4** (Fig. 2) belongs to a simplified series of purine-based PNP transition state inhibitors [19] and has a K_d of 5.5 nM for hPNP, although binding is weaker than that of immucillin-H **3** ($K_d = 6$ pM). In contrast, the substrate inosine has a K_d of 10,000 nM for hPNP [19]. We were interested to replace the purine base of the transition inhibitors with a uracil base to generate a new series of compounds and investigate if they show activity against *Pf*PNP. Therefore uracil containing derivatives of compound **5** were designed, prepared and tested for inhibition against *Pf*PNP. Compound **5** is the general structure for the proposed transition state inhibitor with the purine replaced by uracil. In our study, we prepared a series of inhibitors (**18**–**22** and **24**, **25**) which exhibit an alkyl chain length of two to four carbon atoms between these two nitrogen atoms.

2. Chemistry

2.1. Series *1*

The first series of compounds prepared were barbituric acid derived inhibitors of human uracil phosphorylase. 5-(*m*-Benzyloxy) benzylbarbituric acid (BBB, **1**) and 1-[(2-hydroxyethoxy)methyl]-5-(*m*-benzyloxy)benzylbarbituric acid (BBBA, **2**) were prepared as shown in Scheme 1. Barbituric acid (**6**) was coupled to benzaldehyde or *m*-benzyloxybenaldehyde to give the derivatives **7** and **8** respectively [20]. Products **7** and **8** were used crude as they contained more than 80% product and the removal of unreacted aldehydes proved problematic. The α, β-enone was reduced with sodium borohydride. Work was then carried out to introduce the side chain. Attempts to react compound **1** with 2-acetoxyethyl acetoxymethyl ether were unsuccessful [21]. However the reaction was successfully completed using (2-acetoxyethoxy)methyl bromide following a literature procedure [22]. (2-Acetoxyethoxy)methyl bromide **12** was prepared [23] by stirring acetyl bromide and 1,3-dioxolane together at room temperature, and then separating the required product by distillation at 113 °C. Compound **1** was first silylated using bis(trimethylsilyl)acetamide and then stirred with the (2-acetoxyethoxy)methyl bromide to give the required ester **13**. The ester **13** was deprotected to give the final product **2**.

2.2. Series *2*

The second series of inhibitors, compounds **18**–**22** and **24**, **25**, were prepared as shown in Scheme 2. Uracil was stirred with 1,2-dibromoethane, 1,3-dibromopropane or 1,4-dibromobutane [Br $(CH_2)_nBr$ ($n = 2$–4)] in Cs_2CO_3 in DMF at 40 °C for 2 days. Chromatographic purification was used to separate the final products. The dibromoalkanes could alkylate either N1 or N3 of the uracil. In order to investigate this, NOESY spectra were run on compounds **15**–**17** and **23**. Coupling could be observed for compounds **15**–**17** between the proton of N6 and the protons of alkyl chain (H1′ and H2′), but not for compound **23** (Fig. 3). Therefore, in compound **23**, alkylation had occurred on the undesired N3. Compounds **15**–**17** and **23** were then reacted with pyrrolidine or *l*-prolinol in ethanol at 150 °C under microwave conditions to give the final compounds **18**–**22**, **24** and **25**.

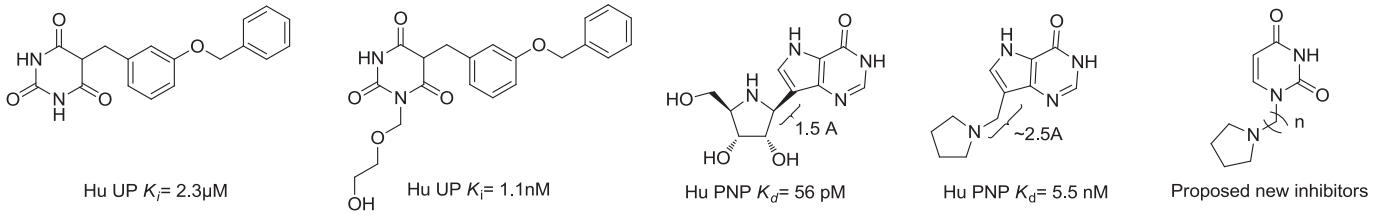

Fig. 2. Four selected known inhibitors and one proposed new inhibitor: (**1**) 5-(*m*-benzyloxy)benzylbarbituric acid, BBB; (**2**) 5-(*m*-benzyloxy)benzylbarbituric acid acyclonucleoside, BBBA; (**3**) Immucillin-H; (**4**) Immucillin-H analogue; (**5**) Proposed new inhibitors, based on compound **4**.

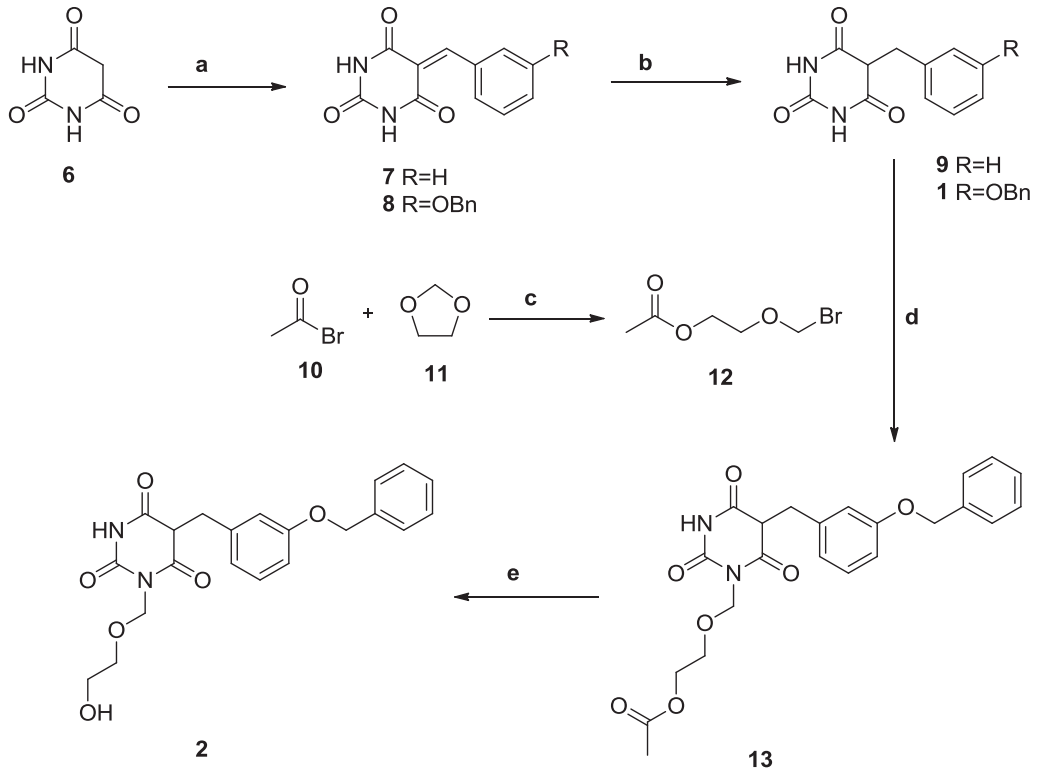

Scheme 1. The synthetic pathway for BBB **1** and BBBA **2**. Reagents and conditions: (a) benzaldehyde or *m*-benzyloxybenzaldehyde, acetic acid, reflux, RT, 85–90%; (b) $NaBH_4$, EtOH, 2 h, RT, 90%; (c) reflux, 70 °C, 29%; (d) (i) chloromethylsilane, hexamethyldisilazane, reflux, 80 °C, overnight, Ar; (ii) (2-acetoxyethoxy)methyl bromide, aluminium chloride, 1,2-dichloroethane, 48 h, RT, Ar, 13%; (e). 0.2 M NaOMe in MeOH, RT, 71%.

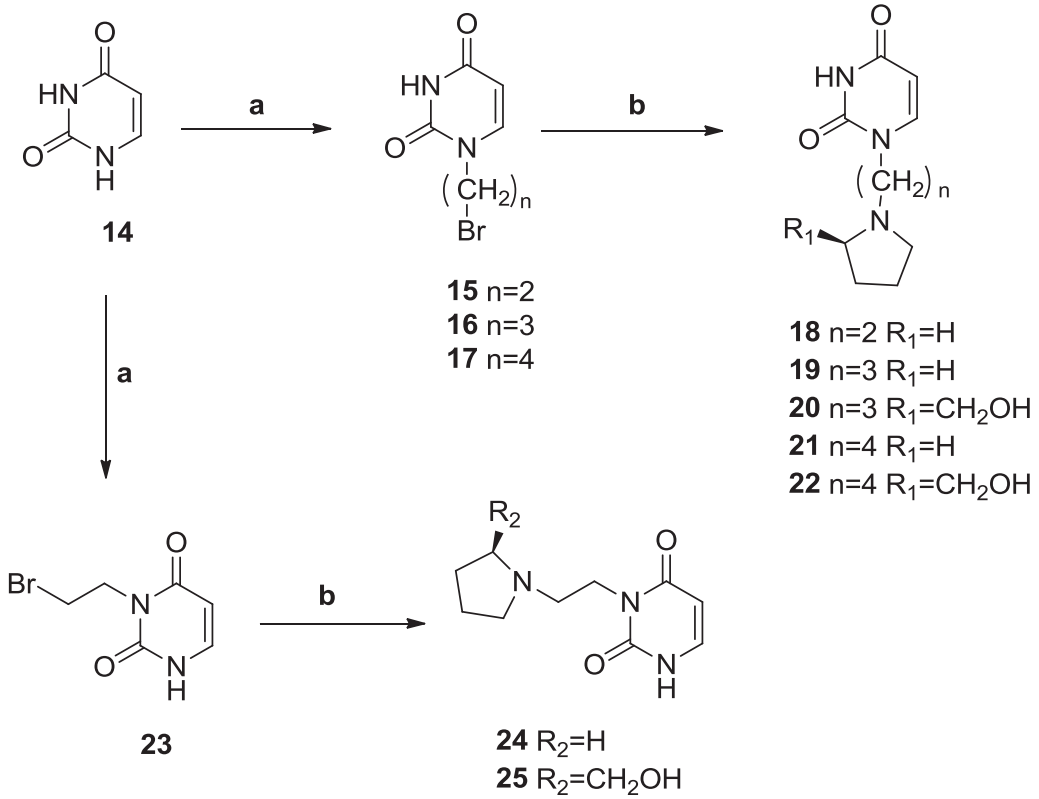

Scheme 2. The synthetic pathway of uracil analogues. Reagents and conditions: (a) $Br(CH_2)_nBr$ ($n = 2$-4), $CsCO_3$, DMF, 40 °C, 48 h, 13–24%; (b) Pyrrolidine or *l*-Prolinol, ethanol, 150 °C, 1 min, microwave, 33–41%.

3. Results and discussion

3.1. Inhibition of *Pf*PNP

Recombinant *Pf*PNP protein [5] was expressed as a soluble protein in *Escherichia coli* BL21 (DE3) cells. Purified recombinant *Pf*PNP appeared as a single band with a subunit molecular weight of approximately 29 kDa in SDS–PAGE. *Pf*PNP assays were performed as previously described [5,6,14]. Kinetic parameters of the His_6 tagged enzyme were similar to those previously reported [5]. The K_m and k_{cat} values were obtained by a non-linear regression fit of the data to the Michaelis–Menten equation (Supplementary data). The values found for inosine were 5.9 μM and 2.1 s^{-1} respectively (Supplementary data). Previous reported values for k_{cat} range from 0.34 to 1.7 s^{-1} whilst the reported K_m value for inosine is 5 μM (Kicska et al. [5] and Lewandowicz et al. [11]).

Compounds **1**, **2**, **9**, **18**–**22**, **24** and **25** were tested for inhibition of *Pf*PNP. The three human UP inhibitors – **1**, **2**, **9** – (Table 1) showed no inhibition of *Pf*PNP even at 1000 μM. Compound **2** was reported to have a K_i against human UP of 1.1 nM [17]. The binding mechanism of these selected human UP inhibitors to human UP has not been elucidated, but was studied in *E. coli* UP [17]. The crystal structure revealed that the large 5-substituent on the barbituric acid could be enclosed in a hydrophobic pocket of *E. coli* UP and the benzyloxy moiety could form additional hydrophobic interactions with Met 234 [17].

The structure of *Pf*PNP was analysed to try and explain the lack of activity of the UP inhibitors. The nucleoside binding site of *Pf*PNP is a hydrophobic pocket where the inosine base is oriented by π-stacking and van der Waals interactions [4]. The flexible benzyloxy moiety of the human UP inhibitors tested may form steric clashes with the binding pocket, if the barbituric acid core binds in a similar manner to purine (Fig. 4E). Additionally, there is a flexible loop in *Pf*PNP which is stabilized by a network of hydrogen bonds with the purine moiety [4]. The large flexible benzyloxy substituents of the barbituric acid might affect this hydrogen bond network and therefore perturb the stabilization of the loop domain. PNP structures also show binding interactions to the ribose ring (for *Pf*PNP, 5′-OH group with His7b from subunit B and Glu184 with the 2′ and 3′ hydroxyl groups). However, compound **4** is active against human PNP, and does not establish ribose–PNP interactions, so these may not have a significant role in its effective inhibition.

Table 1
Evaluation of compounds of series 1 on *Pf*PNP activity.

Compounds	*Pf*PNP IC_{50} (μM)	hUP K_i (μM)
1	>1000	2.3[a]
2	>1000	0.0011[b]
9	>1000	NR[c]

[a] From reference [16].
[b] From reference [17].
[c] Not reported.

Compounds **18**–**22**, **24** and **25** were designed to mimic the transition state inhibitors of PNPs. The *Pf*PNP inhibition assay revealed that they showed reasonable inhibitory activities against *Pf*PNP, with K_i values ranging from 6 μM to 136 μM (Table 2). In particular compounds **24**, **18** and **19** showed good inhibition (K_i = 6 μM, 27 μM and 59 μM respectively).

In order to try and interpret our results, we carried out some molecular modelling. We modeled the inhibitors into the active site of the *Pf*PNP (Fig. 4). Compounds **18** and **24** were superimposed within the active site of the protein 1NW4 [6] (active site between chains A & B), by superposition of the uracil ring and the purine ring of Immucillin-H. The uracil ring was superimposed on the hypoxanthine ring of the Immucillin-H in order to maintain, as far as possible, the H-bonding network, which is almost certainly driving much of the binding energy (Table 3). The pyrrolidine ring could then extend from the base-binding site towards Ser91. This is the residue that binds with the basic nitrogen in Immucillin-H and presumably also the pyrrolidine ring in compound **4**. Hydrogen

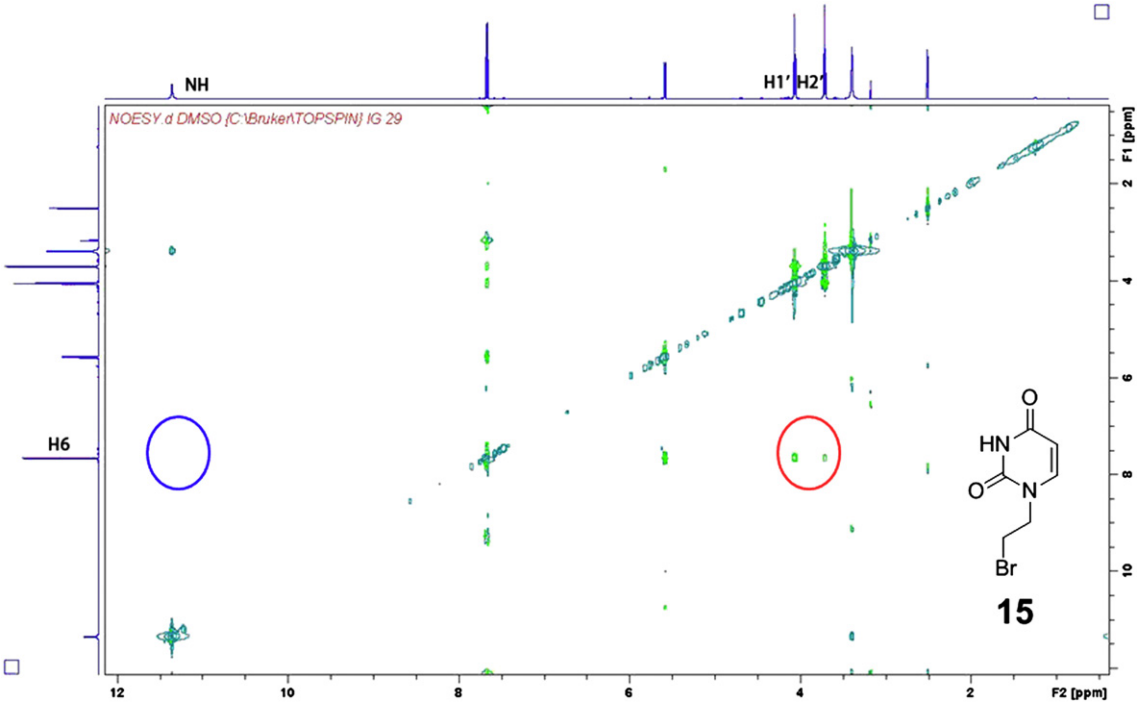

Fig. 3. The identification of compounds **15**–**17** with **23** by NOESY NMR. The coupling between the H6 and the proton of the alkyl chains (H1′ or H2′) is marked in the red circle. (For interpretation of the references to colour in this figure legend, the reader is referred to the web version of this article).

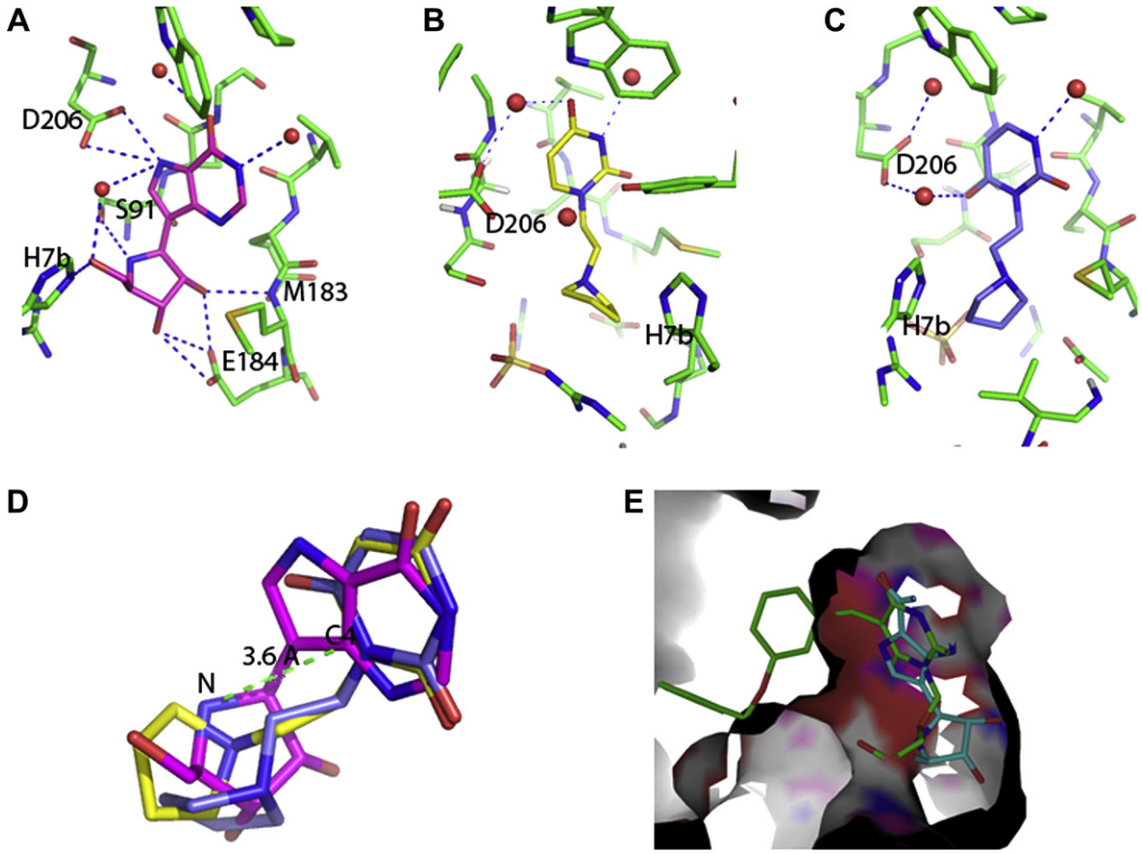

Fig. 4. Computer modelling study of **18** (yellow) and **24** (blue) in the active centre of *Pf*PNP. A. Crystal structure of immucillin-H (magenta) in the active site of *Pf*PNP [6], the hydrogen bonds are shown in the figure. B. The predicted binding mode of compound **18** (yellow) in the active site of PfPNP; C. The predicted binding mode of compound **24** (blue) in the active site of PfPNP; D. Comparison of the predicted binding modes of compounds **18** (yellow), **24** (blue) to Immucillin-H (magenta) in the active centre of *Pf*PNP. The distance between C4 and basic N in immucillin-H was measured to be 3.6 Å. E. The human UP inhibitor BBBA (**2**) (green) was superimposed in the active centre of *Pf*PNP based on the similar binding mode as Immucillin-H (light blue), and the barbituric acid core occupied the position of the purine base. However, the BBBA showed a steric crash in the active centre of *Pf*PNP. (For interpretation of the references to colour in this figure legend, the reader is referred to the web version of this article).

atoms were added to the protein residues and the ligand, and the enzyme–ligand structures were optimized using the Moloc force field [24,25]. For optimization the protein was kept rigid, except for the hydrogens, the ligands and the water molecules within the active site, which were considered flexible (Fig. 4A and B). Whilst this model is speculative, in the absence of structural confirmation, it provides a reasonable explanation of the kinetic data.

The modelling showed that both compounds could fit adequately in the active site and that there is some potential for further inhibitor design. In both cases the uracil base is predicted to be oriented in the nucleoside binding pocket by a π-stacking similar to the purine base of Immucillin-H. The N1 of the uracil base in compound **18** and the N3 of the uracil base in compound **24** roughly superimpose with the C4 of Immucillin-H (Fig. 4C). Additionally the basic nitrogen of the pyrrolidine rings in immucillin-H and compounds **18** and **24** appeared very close to each other. The interactions between the ligands and the *Pf*PNP were compared and are shown in Table 3 and Fig. 4. The interactions between Immucillin-H and *Pf*PNP are from the crystal structure, and for compounds **18** and **24,** from our model.

Table 2
Evaluation of compounds of series 2 on *Pf*PNP and *Plasmodium falciparum* growth *in vitro*.

Compounds	Log *P*[a]	tPSA[a]	*Pf*PNP K_i (IC50) (μM)	EC_{50} (μM)	Atom distance (Å)[b]
18	−0.4	53	27 (141)	>500	3.7
19	−0.3	53	59 (230)	>1000	4.8
20	−0.8	73	136 (712)	375	4.8
21	0.2	53	105 (524)	>1000	6.1
22	−0.4	73	113 (592)	>1000	6.1
24	−0.4	53	6 (42)	>500	3.7
25	−0.9	73	75 (366)	>1000	3.7
Chloroquine				0.03	

[a] Calculated log *P* and tPSA by the software of Chem Draw 12.0.
[b] Calculated atom distance between the N-cationic centre and the N-1 (**18**–**22**) or N-3 (**24** and **25**) atom of the uracil base by Chem Draw 12.0.

Table 3
Interactions between the different compounds and *Pf*PNP.

Immucillin-H	Compound **18**	Compound **24**
H-bond to N7 from D206	H_2O mediated H-bond to O4 from D206	H_2O mediated H-bond to O4 from D206
H-bond to 5′ OH from H7b	H-bond to N3 from H_2O	H-bond to N1 from H_2O
H-bond to 2′ OH from M183		
H-bond to 2′ OH from E184		
H-bond to 3′ OH from E184		
H-bond to basic N from S91		
H_2O mediate H-bond to N7 from 5′ OH		
H-bond to O6 from H_2O		
H-bond to N1 from H_2O		

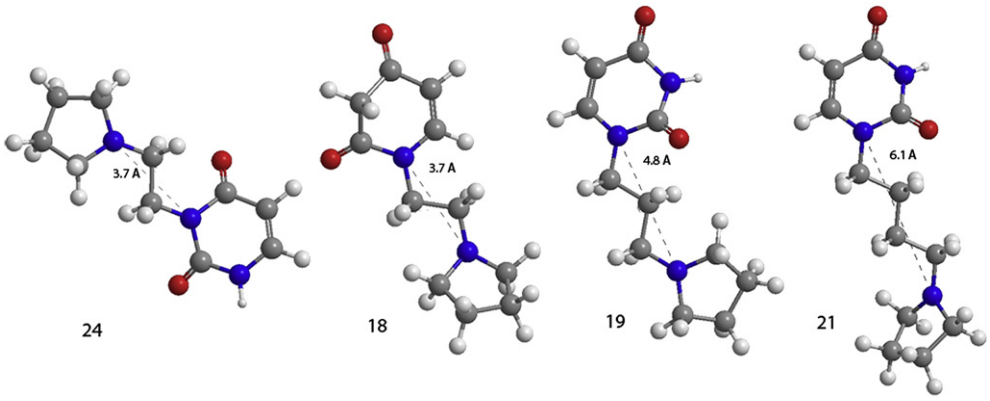

Fig. 5. The distance between the N-cationic centre and the nitrogen of the uracil base in various inhibitors of this study. The distance measured is as follows **18** (3.7 Å), **19** (4.8 Å), **21** (6.1 Å), **24** (3.7 Å). The distance measured for other compounds was **20** = **19**, **22** = **21**, **25** = **24**. Measurements were performed using Chem Draw 12.0.

It is thought that the key factors affecting the binding of the transition state analogues to *Pf*PNP are: (i) the presence of the N-cationic centre of the pyrrolidine ring which binds to and mimics the intermediate oxocarbenium ion; (ii) the relative orientation of the N-cationic centre and the purine ring – the reported optimum distance between the 7-position of the purine and the N appears to be in the range 1.5–3.0 Å; (iii) the presence of the hydroxymethyl substituent on the pyrrolidine ring which can H-bond with the *Pf*PNP [13,19].

We therefore decided to compare the distances between the uracil ring and N-cationic centre of the pyrrolidine ring with activity. The distance was measured from N1 for the N1-substituted derivatives (**18**–**22**) and from the N3 for the N3-subtituted derivatives (**24** and **25**) (Fig. 5 and Table 3). Our modelling showed that the N1 of the uracil base in compound **18** and the N3 of the uracil base in compound **24** roughly superimposed with the C4 of Immucillin-H (Fig. 4C). The corresponding distance for immucillin-H is from the 4-position of the purine ring and is 3.6 Å. There appears to be some relationship between this distance and inhibition of *Pf*PNP. Thus the most potent inhibitors were **18** and **24**, which had a very similar distance to that of immucillin-H; this is also seen in the overlap of predicted inhibitor conformations (Fig. 4D).

The orientation and the presence of hydroxyl groups of the pyrrolidine ring is another factor that affects activity. Analysis of crystal structures of PNPs in general indicates that there are H-bonding interactions between the ribose ring and the protein. The crystal structure of *Pf*PNP-Immucillin-H revealed that the 5′ hydroxyl group of the ribose forms a hydrogen bond with the His7b [4] and the 2′- and 3′-OH groups bind with Glu184 [6]. This is exemplified in compound **4** (K_d of 5.5 nM for hPNP); addition of a hydroxymethyl group to the 5′-position and a hydroxyl to the 3′-position, gives a compound with K_d of 8.5 pM for hPNP [26]. Interestingly in the case of the *Pf*PNP, the crystal structure shows a cavity around the 5′-hydroxyl group, which is not present in the corresponding human enzyme, which may indicate possibilities for selective inhibition. In our case, the hydroxymethyl group actually slightly decreases activity when compared **24** to **25** and **19** to **20**.

3.2. Antiplasmodial activity

Unfortunately none of the compounds showed any significant inhibition of growth of the parasites, even those showing low micromolar K_i values (see Supplementary data). The lack of activity could be due to a number of reasons. One possibility is low cellular permeability, as the compounds are calculated to have a low log *P*. Alternatively the level of enzyme inhibition is insufficient to efficiently deplete PNP activity intracellularly. Furthermore it is not clear if inhibition of human PNP is also required for antiparasitic activity [5,10], as, at least in some circumstances, *Plasmodium* parasites appear to also exploit host enzymes for the conversion of adenosine and inosine into hypoxanthine before translocation across the parasite plasma membrane. In this study, our compounds may not be active against hPNP.

4. Conclusion

*Pf*PNP has been shown to present unique properties and inhibitors of the *Plasmodium* enzyme exhibit antiparasitic activity [5,6,10]. Based on the observation that uridine can be a substrate of the enzyme, we have tested several human uridine phosphorylase inhibitors against *Pf*PNP and designed several new uracil based analogues to mimic the PNP transition state. The results show that while human UP inhibitors are inactive against *Pf*PNP, the uracil based transition state analogues gave significant inhibition with K_i values in the micromolar range. However, these compounds do not have significant antiparasitic activity and therefore are not suitable for further development as antimalarials.

5. Experimental procedures

5.1. Enzyme purification and inhibition assays

The coding sequence of *Pf*PNP was cloned in pET 28a and expression was performed in *E. coli* BL21 (DE3) cells, by induction with 1 mM IPTG at 37 °C for 4 h. Cell pellets were suspended in buffer A (50 mM NaH_2PO_4, pH 8.0, 300 mM NaCl). The cells were lysed by sonication, and the cell extract was cleared by centrifugation at 15,000 rpm for 30 min. The supernatant was loaded onto a nickel affinity chromatography column and was eluted with buffer B (50 mM NaH_2PO_4, pH 8.0, 300 mM NaCl, 25–500 mM imidazole) at 4 °C. Fractions containing purified *Pf*PNP were pooled, desalted on a PD10 column (GE Healthcare) and resuspended in 50 mM NaH_2PO_4, pH 7.5.

Activity was determined in a reaction mixture of final volume 1 ml containing 50 mM NaH_2PO_4, pH 7.5, 2.5 mg xanthine oxidase (60 mU), 2 μg (68.7 nM) *Pf*PNP, and inosine at 25 °C. The reaction was initiated with enzyme and no evidence for two-state inhibition was obtained for any of the compounds tested. In this coupled

assay, inosine is converted to hypoxanthine which is oxidized to uric acid by xanthine oxidase and the reaction is followed spectrophotometrically at 293 nM. Product formation was calculated using the molar extinction coefficient for uric acid: 12.9 mM^{-1} cm^{-1}. k_{cat} and K_m values were calculated by fitting the data obtained at different inosine concentrations (0.5–200 μM) to the Michaelis–Menten equation. IC_{50} values for *Pf*PNP were based on reaction rate measurements with inosine as substrate (25 μM) and variable inhibitor concentrations. For IC_{50} determination, at least five concentrations were tested. K_i values were obtained assuming competitive inhibition and using Dixon plots. Essentially the reciprocal of the reaction velocity is plotted against the concentration of the inhibitor, and the value of K_i is determined from the slope of the plot and the intercept on the *y*-axis. The Dixon plot uses the following equation:

$$\frac{1}{v} = \frac{K_m}{K_i[S]V_{max}}[I] + \frac{1}{V_{max}}\left(1 + \frac{K_m}{[S]}\right)$$

where v = reaction velocity, V_{max} = limiting value of the velocity of the reaction obtained at high substrate concentrations, K_m = Michaelis constant for inosine (5.9 μM), [S] = substrate concentration (25 μM), [I] = inhibitor concentration.

5.2. In vitro assays

In vitro activity against the erythrocytic stages of *P. falciparum* was determined by using an SYBR green assay [27]. The parasite *P. falciparum* 3D7 was cultured using standard methods, and synchronized using 5% sorbitol as previously described. Compounds were dissolved in DMSO at 100 mM and added to 48 h post-synchronization parasite cultures incubated in RPMI 1640 medium with hypoxanthine (150 μM), $NaHCO_3$ (0.2%), gentamycin (12.5 μg/ml), Albumax (0.5%), human serum (2%) and washed human red cells O^+ at 5% haematocrit (0.3% parasitaemia). Chloroquine was used as standard drug. Experiments were carried out at least twice independently and the different concentrations were tested in duplicate. After 48 h of growth, 100 μl of SYBR green I (Molecular Probes) in lysis buffer (Tris 20 mM, pH.7.5, EDTA 5 mM, saponin 0.008%, tritonX-100 0.08%; 0.2 μl of SYBR-green/ml of lysis buffer) was added to each well, and mixed and after 1 h of incubation in the dark at RT, fluorescence was measured with excitation and emission wavelength bands centred at 485 and 530 nm. The percent inhibition of each compound at each concentration was determined. EC_{50} values were calculated from hyperbolic or sigmoidal dose–response curves using Sigmaplot 10.0.

5.3. Modelling

3D structures for compounds **18** and **24** were drawn using Chem3D (ChembridgeSoft, Cambridge, UK). These structures were then manually docked into *Pf*PNP active site (pdb 1NW4 between chains A & B) by superposition with the co-crystallised inhibitor (Immucillin-H) using PyMol (Schrodinger, LLC). Subsequently the inhibitor Immucillin-H was removed and polar hydrogen atoms were added to polar atoms and their positions were minimized using the MAB force field [24,25] as implemented in Moloc (Gerber Molecular Design, Switzerland) with the compounds present in order to obtain a hydrogen-bonding network optimized for ligand binding. Water molecules were kept in the active site during the optimization and protein residues were kept stationary whilst ligand, waters and hydrogen atoms were considered flexible. The optimized binding poses were then inspected using PyMol.

5.4. Chemistry

5.4.1. General

Chemical and solvents were purchased from the Sigma–Aldrich Chemical Company, Fluka, VWR, Acros, Fisher Chemicals and Alfa Aesar. ^1H NMR, ^{13}C NMR and COSY NMR were recorded on a Bruker Avance DPX 500 spectrometer (^1H at 500.1 MHz and ^{13}C at 125.8 MHz). Chemical shift (δ) are expressed in ppm. Signal splitting patters are described as singlet (s), broad singlet (bs), double (d), triplet (t), quarter (q), multiplet (m). Low resolution electrospray (ES) mass spectra were recorded either on a Applied Biosystem Mariner API-TOF biospectrometry Workstation spectrometer or on a Bruker MicroTof mass spectrometer, run in a positive ion mode, using either methanol, methanol/water (95:5), or water/acetonitrile (1:1) + 0.2% formic acid as the mobile phase. High resolution electrospray measurements were performed on a Bruker Daltonics MicrOTOF mass spectrometer. Column-chromatography was carried out using Silica gel 60 from Fluka. Thin layer chromatography (TLC) was carried out on Merck silica gel 60 F254 plates using UV light or PMA for visualization. TLC data are given as the R_f value with the corresponding eluent system specified in brackets.

5.4.2. 5-Benzylidenebarbituric acid (**7**) [23]

Acetic acid (7.5 ml) solution of barbituric acid (128 mg, 1 mmol) and 3-benzylaldehyde (144 mg, 1.2 mmol) was refluxed at 97–100 °C for 2 h. The yellow reaction solution mixture was concentrated to around 3 ml and the resulting yellow suspension left at RT overnight. The solid was separated by filtration, washed with ice-cold methanol (3 × 10 ml) and dried at 110 °C for 2 h. The final product (194 mg, 90%) was yield as a white solid. Reverse phase TLC (50% MeOH/H_2O) R_f = 0.55; LCMS (ES^+): *m*/*z* (%), 217 (100) $[M + H]^+$.

5.4.3. 5-(m-Benzyloxy)benzylidenebarbituric acid (**8**) [16]

Barbituric acid (128 mg, 1 mmol) was coupled with 3-benzyloxy-benzaldehyde (270 mg, 1.2 mmol) following the same procedure of **7**. The final product (273 mg, 85%) is yield as a light yellow solid. Reverse phase TLC (50% MeOH/H_2O) R_f = 0.52; LCMS (ES^+): *m*/*z* (%), 340 (100) $[M + NH_3]^+$, 323 (75) $[M + H]^+$.

5.4.4. 5-Benzylbarbituric acid (**9**) [23]

To a suspension of compound **6** (216 mg, 1 mmol) in ethanol (20 ml) was added $NaBH_4$ (113 mg, 3 mmol). The reaction mixture was stirred at RT for 2 h. The final suspension was filtered and washed with ethanol (20 ml) and DCM to give compound **9** (196 mg, 90%) as a white solid. Reverse phase TLC (50% MeOH/H_2O) R_f = 0.55; ^1H NMR (500 MHz, d^2-H_2O) δ 7.04–7.24 (m, 5H, *H*–Ph and C*H*-3), 3.45 (s, 2H, CH_2); ^{13}C NMR (125 MHz, d^2-H_2O) δ 172.7 (*C4*), 166.5 (*C2*), 153.1 (*C6*), 142.0, 129.95, 128.97, 128.5, 128.4, 128.2, 127.7, 125.6 (*C*–Ph), 89.1 (*C3*), 27.5 (CH_2); LCMS (ES^+): *m*/*z* (%) 219 (100) $[M + H]^+$, 437 (56) $[2M + H]^+$; HRMS (ES^+): calcd for $C_{11}H_{10}N_2O_3$ $[M + H]^+$ 219.0764 *m*/*z*, found 219.0763 *m*/*z*.

5.4.5. 5-(m-Benzyloxy)benzylbarbituric acid (**1**) [16]

Compound **8** (322 mg, 1 mmol) was reacted with $NaBH_4$ in ethanol to give compound (**1**) (290 mg, 90%) as a white solid. Reverse phase TLC (50% MeOH/H_2O) R_f = 0.60; ^1H NMR (500 MHz, d^2-H_2O) δ 7.16–7.32 (m, 5H, *H*–Ph), 7.06 (t, *J* = 7.9 Hz, 1H, *H*–Ph), 6.76 (d, *J* = 7.6 Hz, 1H, *H*–Ph), 6.66 (dd, *J* = 3.4 Hz, 1H, *H*–Ph), 6.56 (s, 1H, *H*–Ph), 4.93 (s, 2H, OCH_2), 3.35 (s, 2H, CH_2); ^{13}C NMR (125 MHz, d^2-H_2O) δ 166.3 (*C4*), 157.6 (*C2*), 153.0 (*C6*), 143.91 (*C*–Ph), 136.8, 129.4, 128.6, 128.0, 127.5, 121.2, 113.8, 113.0 (*C*–Ph), 88.8 (*C3*), 70.1 (OCH_2), 27.34 (CH_2); LCMS (ES^+): *m*/*z* (%) 325 (100) $[M + H]^+$, 649 (25) $[2M + H]^+$; HRMS (ES^+): calcd for $C_{18}H_{17}N_2O_4$ $[M + H]^+$ 325.1183 *m*/*z*, found 325.1185 *m*/*z*.

*5.4.6. (2-Acetoxyethoxy)methyl bromide (**12**) [23]*

Acetyl bromide (8.32 g, 0.0676 mol) was added dropwise to 1,3-dioxolane (5.01 g, 0.0676 mol) with stirring at RT. After addition of 1/3 of the acetyl bromide, the temperature was raised to reflux (70 °C) and the remaining acetyl bromide was added over a 15 min period. After refluxing for 4 h, the solution was subjected to fractional distillation. At 113 °C, the product (3.8 g, 29%) was distilled as a liquid. ^{1}H NMR (500 MHz, d^1-$CHCl_3$) δ 5.66 (s, 2H, CH_2), 4.23 (t, 2H, CH_2), 3.82 (m, 2H, CH_2), 2.03 (s, 2H, CH_3); ^{13}C NMR (125 MHz, d^1-$CHCl_3$) δ 170.6 (*C*O), 75.7, 75.6 (*C*H_2), 69.3, 69.24, 69.17, 69.1 (*C*H_2), 62.3, 62.12, 62.09 (*C*H_2), 20.7 (*C*H_3).

*5.4.7. 1-[(2-Acetoxyethoxy)methyl]-5-(m-benzyloxy) benzylbarbituric acid (**13**) [23]*

Compound **1** (2 g, 6.17 mmol) and chlorotrimethylsilane (1.6 ml, 18 mmol) were heated in hexamethyldisilazane (HMDS) (100 ml) and refluxed overnight (75–80 °C) in Ar. The excess HMDS was removed by evaporation (100 °C) and the resulting crystalline persilylated compound **1** was dissolved in dry 1,2-dichloroethane (20 ml). Compound **12** (1.2 g, 6.17 mmol) and a catalytic amount of anhydrous aluminium chloride (40 mg) were added to the reaction, and the reaction mixture was allowed to stir for 48 h at RT under anhydrous condition. The reaction mixture was then cooled and carefully neutralized (pH = 7) with a saturated Na_2CO_3. The organic layer was separated and the aqueous phase was extracted with chloroform (3 × 100 ml). The organic layer and extracts were combined and dried over anhydrous $MgSO_4$. The dried organic layer was evaporated to dryness and the resulting residue was dissolved in a minimal amount of DCM and applied to a silica gel column, The column was eluted with 2% MeOH/DCM to give compound **13** (352 mg, 13%) as a white solid. TLC (10% MeOH/DCM) R_f = 0.43; LCMS (ES$^+$): *m*/*z* (%) 458 (100) $[M + NH_3]^+$, 441 (70) $[M + H]^+$; HRMS (ES$^+$): calcd for $C_{23}H_{25}N_2O_7$ $[M + H]^+$ 441.1656 *m*/*z*, found 441.1654 *m*/*z*.

*5.4.8. 1-[(2-Hydroxyethoxy)methyl]-5-(m-benzyloxy) benzylbarbituric acid (**2**) [23]*

The ester **13** (250 mg, 0.57 mmol) was dissolved in a solution of 0.2 M sodium methoxide in MeOH. The reaction was stirred at RT until the disappearance of the starting ester which was observed by TLC. The solution was neutralized with Dowex ion exchange resin to pH. 6.0. The residue was filtered and washed twice with MeOH. The MeOH was evaporated to afford a crude residue, which was eluted through a reverse phase column to give the final compound **2** (156 mg, 71%) as a white solid. Reverse TLC (50% MeOH/H_2O) R_f = 0.38; ^{1}H NMR (500 MHz, d^4-MeOH) δ 7.27–7.43 (m, 5H, *H*–Ph), 7.08 (t, *J* = 7.8 Hz, 1H, *H*–Ph), 6.95 (d, *J* = 1.5 Hz, 1H, *H*–Ph), 6.89 (d, *J* = 7.6 Hz, 1H, *H*–Ph), 6.70 (dd, *J* = 3.3 Hz, 1H, *H*–Ph), 5.36 (s, 2H, NCH_2), 5.04 (s, 2H, OCH_2), 3.60–3.69 (m, 6H, OCH_2, OCH_2 and CH_2); ^{13}C NMR (125 MHz, d^4-MeOH) δ 166.6, 166.3 (*C4*), 160.1 (*C2*), 154.6 (*C6*), 146.2 (*C*–Ph), 139.2 (*C*–Ph), 129.6, 129.4, 128.7, 128.6, 122.1, 115.6, 112.8 (*C*–Ph), 89.4 (*C3*), 71.6, 71.2, 70.8 (NCH_2, OCH_2 and OCH_2), 62.2 (OCH_2), 30.0 (CH_2); LCMS (ES$^+$): *m*/*z* (%) 416 (100) $[M + NH_3]^+$, 399 (53) $[M + H]^+$; HRMS (ES$^+$): calcd for $C_{21}H_{23}N_2O_6$ $[M + H]^+$ 399.1551 *m*/*z*, found 399.1539 *m*/*z*.

*5.4.9. General procedures for **15**–**17** and **23***

Uracil (10 mmol, 1 eq) and Br(CH_2)$_n$Br (*n* = 2–4) (10 mmol, 1 eq) were stirred in DMF (50 ml) with Cs_2CO_3 (10 mmol, 1 eq) at 40 °C for 48 h. The residue was evaporated to remove DMF and purified by chromatography with 5% MeOH/DCM.

*5.4.10. 1-(2-Bromoethyl)uracil (**15**) [28]*

Uracil (1.12 g, 10 mmol) and 1,2-dibromoethane (0.85 ml, 10 mmol) reacted and yield compound **15** (280 mg, 13%) as a white solid. TLC (10% MeOH/DCM) R_f = 0.31; ^{1}H NMR (500 MHz, d^6-DMSO) δ 11.35 (s, 1H, N*H*), 7.66 (d, *J* = 7.8 Hz, 1H, *H6*), 5.58 (dd, *J* = 3.3 Hz, 1H, *H5*), 4.06 (t, *J* = 6.3 Hz, 2H, NCH_2), 3.71 (t, *J* = 6.3 Hz, 2H, CH_2); ^{13}C NMR (125 MHz, d^6-DMSO) δ 163.6 (*C4*), 150.8 (*C2*), 145.8 (*C6*), 100.7 (*C5*), 48.8 (NCH_2), 30.7 (CH_2); LCMS (ES$^+$): *m*/*z* (%) 139 (100) $[M - HBr]^-$, 218 (33) $[M + H]^+$.

*5.4.11. 1-(3-Bromopropyl)uracil (**16**)*

Uracil (1.12 g, 10 mmol) and 1,3-dibromopropane (1 ml, 10 mmol) reacted and yield compound **16** 550 mg (24%) as a white solid. TLC (10% MeOH/DCM) R_f = 0.33; ^{1}H NMR (500 MHz, d^6-DMSO) δ 11.26 (s, 1H, N*H*), 7.62 (d, *J* = 7.8 Hz, 1H, *H6*), 5.56 (dd, *J* = 3.3 Hz, 1H, *H5*), 3.77 (t, *J* = 6.9 Hz, 2H, NCH_2), 3.53 (t, *J* = 6.6 Hz, 2H, BrCH_2), 2.13 (qt, *J* = 6.7 Hz, 2H, CH_2); ^{13}C NMR (125 MHz, d^6-DMSO) δ 163.7 (*C4*), 150.9 (*C2*), 145.6 (*C6*), 101.0 (*C5*), 46.5 (NCH_2), 31.32 (BrCH_2), 31.29 (CH_2); LCMS (ES$^+$): *m*/*z* (%) 153 (100) $[M - HBr]^-$, 232 (24) $[M + H]^+$.

*5.4.12. 1-(4-Bromobutyl)uracil (**17**)*

Uracil (1.12 g, 10 mmol) and 1,4-dibromobutane (1.18 ml, 10 mmol) reacted and yield compound **17** (440 mg, 18%) as a white solid. TLC (10% MeOH/DCM) R_f = 0.33; ^{1}H NMR (500 MHz, d^6-DMSO) δ 11.26 (s, 1H, N*H*), 7.76 (d, *J* = 7.8 Hz, 1H, *H6*), 5.56 (d, *J* = 7.8 Hz, 1H, *H5*), 3.69 (t, *J* = 6.8 Hz, 2H, NCH_2), 3.56 (t, *J* = 6.5 Hz, 2H, BrCH_2), 1.78 (qt, *J* = 6.9 Hz, 2H, CH_2), 1.69 (qt, *J* = 5.8 Hz, 2H, CH_2); ^{13}C NMR (125 MHz, d^6-DMSO) δ 163.7 (*C4*), 150.9 (*C2*), 145.6 (*C6*), 100.9 (*C5*), 46.5 (NCH_2), 34.5 (BrCH_2), 29.1 (CH_2), 27.2 (CH_2); LCMS (ES$^+$): *m*/*z* (%) 247 (99) $[M + H]^+$, 249 (100) $[M + 3H]^+$.

*5.4.13. 3-(2-Bromoethyl)uracil (**23**)*

Uracil (1.12 g, 10 mmol) and 1,2-dibromoethane (0.85 ml, 10 mmol) reacted and yield compound **23** (325 mg, 15%) as a white solid. TLC (10% MeOH/DCM) R_f = 0.25; ^{1}H NMR (500 MHz, d^6-DMSO) δ 7.70 (d, *J* = 6.6 Hz, 1H, *H6*), 5.98 (d, *J* = 6.6 Hz, 1H, *H5*), 4.69 (t, *J* = 8.5 Hz, 2H, BrCH_2), 4.16 (t, *J* = 8.5 Hz, 2H, NCH_2); ^{13}C NMR (125 MHz, d^6-DMSO) δ 160.5, 160.3 (*C4*), 154.8 (*C2*), 107.3 (*C6*), 100.7, 100.0 (*C5*), 66.6 (Br*C*), 42.3 (N*C*); LCMS (ES$^+$): *m*/*z* (%) 139 (100) $[M - HBr]^-$, 218 (5) $[M + H]^+$.

*5.4.14. General procedures for **18**–**22** and **24**, **25***

Compounds **15**–**17** and **23** (1 mmol, 1 eq) were stirred with pyrrolidine or *l*-prolinol (1 mmol, 1 eq) at 150 °C in ethanol under microwaves irradiation for 1 min. Then ethanol was evaporated and the residue was purified by chromatography in 20% methanol/DCM to give the final product.

*5.4.15. 1-((2-Pyrrolidine-1-yl)-ethyl)uracil (**18**)*

Compound **15** (217 mg, 1 mmol) reacted with pyrrolidine (83 μl, 1 mmol) to give product **18** (68 mg, 33%) as a light yellow solid. TLC (20% MeOH/DCM) R_f = 0.02; ^{1}H NMR (500 MHz, d^4-MeOH) δ 7.64 (d, *J* = 7.8 Hz, 1H, *H6*), 5.68 (d, *J* = 7.8 Hz, 1H, *H5*), 3.98 (t, *J* = 6.4 Hz, 2H, NCH_2), 2.99 (t, *J* = 5.6 Hz, 2H, NCH_2), 2.84 (m, 4H, CH_2NCH_2), 1.90 (m, 4H, CH_2CH_2); ^{13}C NMR (125 MHz, d^4-MeOH) δ 166.8 (*C4*), 153.0 (*C2*), 147.3 (*C6*), 102.4 (*C5*), 55.3 (NCH_2), 55.2 (NCH_2), 46.7 (CH_2NCH_2), 24.29 (CH_2CH_2); LCMS (ES$^+$): *m*/*z* (%) 210 (100) $[M + H]^+$; HRMS (ES$^+$): calcd for $C_{10}H_{16}N_3O_2$ $[M + H]^+$ 210.1237 *m*/*z*, found 210.1248 *m*/*z*.

*5.4.16. 1-((3-Pyrrolidine-1-yl)-propyl)uracil (**19**)*

Compound **16** (230 mg, 1 mmol) reacted with pyrrolidine (83 μl, 1 mmol) to give product **19** (82 mg, 37%) as a light yellow solid. TLC (20% MeOH/DCM) R_f = 0.03; ^{1}H NMR (500 MHz, d^4-MeOH) δ 7.62 (d, *J* = 7.8 Hz, 1H, *H6*), 5.66 (d, *J* = 7.8 Hz, 1H, *H5*), 3.82 (t, *J* = 7.1 Hz, 2H, NCH_2), 2.54–2.60 (m, 6H, NCH_2 and CH_2NCH_2), 1.93 (qt, *J* = 7.3 Hz, 2H, CH_2 and CH_2CH_2); ^{13}C NMR δ (125 MHz, d^4-MeOH) 166.9 (*C4*), 152.9 (*C2*), 147.4 (*C6*), 102.2 (*C5*), 54.9 (NCH_2), 54.04

(NCH_2), 48.05 (NCH_2), 28.82 (CH_2), 24.25 (CH_2CH_2); LCMS (ES^+): *m/z* (%) 224 (100) $[M+H]^+$; HRMS (ES^+): calcd for $C_{11}H_{18}N_3O_2$ $[M+H]^+$ 224.1394 *m/z*, found 224.1386 *m/z*.

*5.4.17. 1-((3-(l-Prolinol)-1-yl)-propyl)uracil (**20**)*

Compound **16** (230 mg, 1 mmol) reacted with *l*-prolinol (100 μl, 1 mmol) to give product **20** (88 mg, 35%) as a light yellow solid. TLC (20% MeOH/DCM) $R_f = 0.03$; ^1H NMR (500 MHz, d^4-MeOH) δ 7.68 (d, $J = 7.8$ Hz, 1H, *H6*), 5.68 (d, $J = 7.8$ Hz, 1H, *H5*), 3.60–3.69 (m, 2H, NCH_2), 3.81–3.94 (m, 2H, CH_2), 3.33 (qt, $J = 1.6$ Hz, 1H, NCH*H*), 3.17–3.22 (m, 1H, NC*H*H), 3.01–3.06 (m, 1H, C*H*), 2.64–2.75 (m, 2H, NCH*H* and NC*H*H), 2.01–2.09 (m, 3H, $NCCH_2$ and C*H*H), 1.74–1.95 (m, 3H, CH_2 and C*H*H); ^{13}C NMR (125 MHz, d^4-MeOH) δ 166.9 (*C4*), 152.9 (*C2*), 147.6 (*C6*), 102.1 (*C5*), 67.5 (CH), 64.8 (OCH_2), 55.3 (NCH_2), 53.4 (NCH_2), 48.0 (NCH_2), 28.7 (CH_2), 28.6 (CH_2), 23.7 (CH_2); LCMS (ES^+): *m/z* (%) 254 (100) $[M+H]^+$; HRMS (ES^+): calcd for $C_{12}H_{20}N_3O_3$ $[M+H]^+$ 254.1499 *m/z*, found 254.1500 *m/z*.

*5.4.18. 1-((4-Pyrrolidine-1-yl)-butyl)uracil (**21**)*

Compound **17** (246 mg, 1 mmol) reacted with pyrrolidine (83 μl, 1 mmol) to give product **21** (97 mg, 41%) as a light yellow solid. TLC (20% MeOH/DCM) $R_f = 0.05$; ^1H NMR (500 MHz, d^4-MeOH) δ 7.63 (d, $J = 7.8$ Hz, 1H, *H6*), 5.67 (d, $J = 7.8$ Hz, 1H, *H5*), 3.79 (t, $J = 7.2$ Hz, 2H, NCH_2), 2.68–2.70 (m, 4H, CH_2NCH_2), 2.63 (t, 2H, NCH_2), 1.82–1.89 (m, 4H, CH_2CH_2), 1.73 (qt, $J = 7.4$ Hz, 2H, CH_2), 1.58–1.64 (m, 2H, CH_2); ^{13}C NMR (125 MHz, d^4-MeOH) δ 167.0 (*C4*), 153.0 (*C2*), 147.3 (*C6*), 102.3 (*C5*), 56.8 (CH_2NCH_2), 55.0 (NCH_2), 28.0 (CH_2), 26.13 (CH_2), 24.17 (CH_2); LCMS (ES^+): *m/z* (%) 238 (100) $[M+H]^+$; HRMS (ES^+): calcd for $C_{12}H_{20}N_3O_2$ $[M+H]^+$ 238.1550 *m/z*, found 238.1561 *m/z*.

*5.4.19. 1-((4-(l-Prolinol)-1-yl)-butyl)uracil (**22**)*

Compound **17** (246 mg, 1 mmol) reacted with *l*-prolinol (100 μl, 1 mmol) to give product **22** (106 mg, 40%) as a light yellow solid. TLC (20% MeOH/DCM) $R_f = 0.06$; ^1H NMR (500 MHz, d^4-MeOH) δ 7.61 (d, $J = 7.8$ Hz, 1H, *H6*), 5.67 (d, $J = 7.8$ Hz, 1H, *H5*), 3.79 (t, $J = 7.2$ Hz, 2H, NCH_2), 3.60 (dd, $J = 5.2$ Hz, 1H, OCH*H*), 3.50 (dd, $J = 5.6$ Hz, 1H, OC*H*H), 3.16–3.20 (m, 1H, NC*H*H), 2.93–2.98 (m, 1H, NC*H*H), 2.60–2.65 (m, 1H, C*H*), 2.36–2.42 (m, 1H, NCH*H*), 2.31 (q, $J = 8.7$ Hz, 1H, NCH*H*), 1.91–2.00 (m, 1H, C*H*H), 1.65–1.84 (m, 5H, CH*H*, CH_2 and CH_2), 1.53–1.62 (m, 2H, CH_2); ^{13}C NMR (125 MHz, d^4-MeOH) δ 166.9 (*C4*), 152.9 (*C2*), 147.3 (*C6*), 102.3 (*C5*), 67.94 (CH), 64.91 (OCH_2), 56.2 (NCH_2), 55.5 (NCH_2), 49.6 (NCH_2), 28.8 (CH_2), 26.2 (CH_2), 26.2 (CH_2), 23.7 (CH_2); LCMS (ES^+): *m/z* (%) 268 (100) $[M+H]^+$.

*5.4.20. 3-((2-Pyrrolidine-1-yl)-ethyl)uracil (**24**)*

Compound **23** (217 mg, 1 mmol) reacted with pyrrolidine (83 μl, 1 mmol) to give product **24** (81 mg, 39%) as a light yellow solid. TLC (20% MeOH/DCM) $R_f = 0.02$; ^1H NMR (500 MHz, d^4-MeOH) δ 7.41 (d, $J = 7.6$ Hz, 1H, *H6*), 5.72 (d, $J = 7.6$ Hz, 1H, *H5*), 4.16 (t, $J = 6.6$ Hz, 2H, NCH_2), 3.01 (t, $J = 6.6$ Hz, 2H, NCH_2), 2.95 (m, 4H, CH_2NCH_2), 1.92 (m, 4H, CH_2CH_2); ^{13}C NMR (125 MHz, d^4-MeOH) δ 166.2 (*C4*), 153.6 (*C2*), 142.0 (*C6*), 101.4 (*C5*), 55.4 (NCH_2), 54.3 (CH_2NCH_2), 39.2 (CH_2), 24.15 (CH_2); LCMS (ES^+): *m/z* (%) 210 (100) $[M+H]^+$; HRMS (ES^+): calcd for $C_{10}H_{16}N_3O_2$ $[M+H]^+$ 210.1237 *m/z*, found 210.1245 *m/z*.

*5.4.21. 3-((2-(l-Prolinol)-1-yl)-ethyl)uracil (**25**)*

Compound **23** (217 mg, 1 mmol) reacted with *l*-prolinol (100 μl, 1 mmol) to give product **25** (78 mg, 33%) as a light yellow solid. TLC (20% MeOH/DCM) $R_f = 0.02$; ^1H NMR (500 MHz, d^4-MeOH) δ 7.44 (d, $J = 7.6$ Hz, 1H, *H6*), 5.72 (d, $J = 7.6$ Hz, 1H, *H5*), 4.10–4.15, 4.19–4.24 (m, 2H, NCH_2), 3.62 (m, 2H, OCH_2), 3.52 (m, 1H, NCH*H*), 3.38 (m, 1H, NC*H*H), 3.07 (m, 1H, C*H*), 2.86–2.91 (m, 1H, NCH*H*), 2.78–2.83 (m, 1H, NC*H*H), 2.04–2.13 (m, 1H, C*H*H), 1.92–1.99 (m, 1H, C*H*H), 1.83–1.89 (m, 1H, CH*H*), 1.73–1.80 (m, 1H, CH*H*); ^{13}C NMR (125 MHz, d^4-MeOH) δ 166.1 (*C4*), 153.5 (*C2*), 142.1 (*C6*), 101.4 (*C5*), 68.7 (CH), 63.0 (OCH_2), 55.8 (NCH_2), 53.3 (NCH_2), 39.1 (NCH_2), 28.2 (CH_2), 23.8 (CH_2); LCMS (ES^+): *m/z* (%) 240 (100) $[M+H]^+$; HRMS (ES^+): calcd for $C_{11}H_{18}N_3O_3$ $[M+H]^+$ 240.1343 *m/z*, found 240.1346 *m/z*.

Acknowledgements

Financial support for this research came from the Plan Nacional (SAF2007-62596), the RICET FIS Network (RD06/0021), the Junta de Andalucía (CVI-199) and the European Union (ANTIMAL contract no. LSHP-CT-2005-018834). The authors also want to thank Gina MacKay for HRMS.

Appendix. Supplementary data

Supplementary data associated with this article can be found in the online version, at doi:10.1016/j.ejmech.2010.08.026.

References

[1] B. Greenwood, T. Mutabingwa, Malaria in 2002, Nature 415 (2002) 670–672.
[2] Africa Malaria Report, 2003. Available from: http://www.rbm.who.int/amd2003/amr2003/amr2003/amr_toc.htm.
[3] I. Bathurst, C. Hentschel, Medicines for malaria venture: sustaining antimalarial drug development, Trends Parasitol. 22 (2006) 301–307.
[4] C. Schnick, M.A. Robien, A.M. Brzozowski, E.J. Dodson, G.N. Murshudov, L. Anderson, J.R. Luft, C. Mehlin, W.G.J. Hol, J.A. Brannigan, et al., Structures of *Plasmodium falciparum* purine nucleoside phosphorylase complexed with sulfate and its natural substrate inosine, Acta Crystallogr., Sect. D 61 (2005) 1245–1254.
[5] G.A. Kicska, P.C. Tyler, G.B. Evans, R.H. Furneaux, K. Kim, V.L. Schramm, Transition state analogue inhibitors of purine nucleoside phosphorylase from *Plasmodium falciparum*, J. Biol. Chem. 277 (2002) 3219–3225.
[6] W.X. Shi, L.M. Ting, G.A. Kicska, A. Lewandowicz, P.C. Tyler, G.B. Evans, R.H. Furneaux, K. Kim, S.C. Almo, V.L. Schramm, *Plasmodium falciparum* purine nucleoside phosphorylase: crystal structures, immucillin inhibitors, and dual catalytic function, J. Biol. Chem. 279 (2004) 18103–18106.
[7] A. Lewandowicz, V.L. Schramm, Transition state analysis for human and *Plasmodium falciparum* purine nucleoside phosphorylases, Biochemistry 43 (2004) 1458–1468.
[8] A. Chaikuad, R.L. Brady, Conservation of structure and activity in *Plasmodium* purine nucleoside phosphorylases, BMC Struct. Biol. 9 (2009) 42.
[9] D.C. Madrid, L.M. Ting, K.L. Waller, V.L. Schramm, K. Kim, *Plasmodium falciparum* purine nucleoside phosphorylase is critical for viability of malaria parasites, J. Biol. Chem. 283 (2008) 35899–35907.
[10] G.A. Kicska, P.C. Tyler, G.B. Evans, R.H. Furneaux, V.L. Schramm, K. Kim, Purine-less death in *Plasmodium falciparum* induced by immucillin-H, a transition state analogue of purine nucleoside phosphorylase, J. Biol. Chem. 277 (2002) 3226–3231.
[11] A. Lewandowicz, E.A.T. Ringia, L.M. Ting, K. Kim, P.C. Tyler, G.B. Evans, O.V. Zubkova, S. Mee, G.F. Painter, D.H. Lenz, et al., Energetic mapping of transition state analogue interactions with human and *Plasmodium falciparum* purine nucleoside phosphorylases, J. Biol. Chem. 280 (2005) 30320–30328.
[12] P.C. Kline, V.L. Schramm, Pre-steady-state transition-state analysis of the hydrolytic reaction catalyzed by purine nucleoside phosphorylase, Biochemistry 34 (1995) 1153–1162.
[13] E.A.T. Ringia, P.C. Tyler, G.B. Evans, R.H. Furneaux, A.S. Murkin, V.L. Schramm, Transition state analogue discrimination by related purine nucleoside phosphorylases, J. Am. Chem. Soc. 128 (2006) 7126–7127.
[14] L.M. Ting, W.X. Shi, A. Lewandowicz, V. Singh, A. Mwakingwe, M.R. Birck, E.A.T. Ringia, G. Bench, D.C. Madrid, P.C. Tyler, et al., Targeting a novel *Plasmodium falciparum* purine recycling pathway with specific immucillins, J. Biol. Chem. 280 (2005) 9547–9554.
[15] S. Cha, Development of inhibitors of pyrimidine metabolism, Yonsei Med. J. 30 (1989) 315–326.
[16] D.J. Guerin, D. Mazeas, M.S. Musale, F.N.M. Naguib, O.N. Al Safarjalani, M.H. el Kouni, R.P. Panzica, Uridine phosphorylase inhibitors: chemical modification of benzyloxybenzyl-barbituric acid and its effects on URDPASE inhibition, Bioorg. Med. Chem. Lett. 9 (1999) 1477–1480.
[17] W.M. Bu, E.C. Settembre, M.H. el Kouni, S.E. Ealick, Structural basis for inhibition of *Escherichia coli* uridine phosphorylase by 5-substituted acyclouridines, Acta Crystallogr., Sect. D 61 (2005) 863–872.
[18] J.M. Mason, A.S. Murkin, L. Li, V.L. Schramm, G.J. Gainsford, B.W. Skelton, A beta-fluoroamine inhibitor of purine nucleoside phosphorylase, J. Med. Chem. 51 (2008) 5880–5884.
[19] K. El Bissati, R. Zufferey, W.H. Witola, N.S. Carter, B. Ullman, C. Ben Mamoun, The plasma membrane permease PfNT1 is essential for purine salvage in the human malaria parasite *Plasmodium falciparum*, Proc. Natl. Acad. Sci. U.S.A. 103 (2006) 9286–9291.

[20] B.S. Jursic, E.D. Stevens, Mono C-alkylation and mono C-benzylation of barbituric acids through zinc/acid reduction of acyl, benzylidene, and alkylidene barbiturate intermediates, Tetrahedron Lett. 44 (2003) 2203–2210.
[21] A. Rosowsky, S.H. Kim, M. Wick, Synthesis and antitumor activity of an acyclonucleoside derivative of 5-fluorouracil, J. Med. Chem. 24 (1981) 1177–1181.
[22] G.F. Orr, D.L. Musso, G.E. Boswell, J.L. Kelley, S.S. Joyner, S.T. Davis, D.P. Baccanari, Inhibition of uridine phosphorylase: synthesis and structure–activity relationships of aryl-substituted 5-benzyluracils and 1-[(2-hydroxyethoxy)methyl]-5-benzyluracils, J. Med. Chem. 38 (1995) 3850–3856.
[23] D.L. Levesque, E.C. Wang, D.C. Wei, C.C. Tzeng, R.P. Panzica, F.N.M. Naguib, M.H. Elkouni, Synthesis of a new class of uridine phosphorylase inhibitors, J. Heterocycl. Chem. 30 (1993) 1399–1404.
[24] P.R. Gerber, K. Muller, MAB, a generally applicable molecular force field for structure modelling in medicinal chemistry, J. Comput. Aided Mol. Des. 9 (1995) 251–268.
[25] P.R. Gerber, Charge distribution from a simple molecular orbital type calculation and non-bonding interaction terms in the force field MAB, J. Comput. Aided Mol. Des. 12 (1998) 37–51.
[26] E.A. Taylor, K. Clinch, P.M. Kelly, L. Li, G.B. Evans, P.C. Tyler, V.L. Schramm, Acyclic ribooxacarbenium ion mimics as transition state analogues of human and malarial purine nucleoside phosphorylases, J. Am. Chem. Soc. 129 (2007) 6984–6985.
[27] M. Smilkstein, N. Sriwilaijaroen, J.X. Kelly, P. Wilairat, M. Riscoe, Simple and inexpensive fluorescence-based technique for high-throughput antimalarial drug screening, Antimicrob. Agents Chemother. 48 (2004) 1803–1806.
[28] B. Lohse, S. Hvilsted, R.H. Berg, P.S. Ramanujam, *N*-1-alkylated pyrimidine films as a new potential optical data storage medium, Chem. Mater. 18 (2006) 4808–4816.